Mathematical Modelling and Analysis
Volume 24, Issue 4, 598–616, 2019
https://doi.org/10.3846/mma.2019.036

http://mma.vgtu.lt
ISSN: 1392-6292
eISSN: 1648-3510

Numerical Analysis of Liquid-Solid Adsorption Model

Teresė Leonavičienė, Raimondas Čiegis, Edita Baltrėnaitė and Valeriia Chemerys

Vilnius Gediminas Technical University
Saulėtekio al. 11, LT-10223 Vilnius, Lithuania
E-mail(*corresp.*): terese.leonaviciene@vgtu.lt
E-mail: raimondas.ciegis@vgtu.lt
E-mail: edita.baltrenaite@vgtu.lt
E-mail: valeriia.chemerys@vgtu.lt

Received April 3, 2019; revised September 26, 2019; accepted October 1, 2019

Abstract. In this paper, the numerical algorithms for solution of pore volume and surface diffusion model of adsorption systems are constructed and investigated. The approximation of PDEs is done by using the finite volume method for space derivatives and ODE15s solvers for numerical integration in time. The analysis of adaptive in time integration algorithms is presented. The main aim of this work is to analyze the sensitivity of the solution with respect to the main parameters of the mathematical model. Such a control analysis is done for a linearized and normalized mathematical model. The obtained results are compared with simulations done for a full nonlinear mathematical model.

Keywords: numerical algorithms, finite volume method, adsorption models, sensitivity analysis.

AMS Subject Classification: 65N08; 65N12; 65N22; 35Q92.

1 Introduction

It is well-known that during recent years the environmental pollution questions become a very important issue. The strict environmental requirements encourage to reduce environmental pollution during the industrial processes. The manufacturers look for technologies enabling with low-costs to effectively remove harmful substances. They apply different methods or chemicals.

Adsorption is one of the methods widely used for the removal of pollutants from water. Adsorption is considered as a better and economical alternative

Copyright © 2019 The Author(s). Published by VGTU Press
This is an Open Access article distributed under the terms of the Creative Commons Attribution License (http://creativecommons.org/licenses/by/4.0/), which permits unrestricted use, distribution, and reproduction in any medium, provided the original author and source are credited.

to other conventional methods (e.g. reverse osmosis, coagulation, flocculation, flotation, chemical precipitation etc), because of removal of potentially toxic elements (PTEs) at low concentrations (less than 100 mg/l), flexibility in design and operation. In general adsorption is one of the main surface phenomena. During the interaction of two different phases (fluid and solid) the higher concentration at the solid surface implies adsorption process and the change in concentration in the interfacial layer is obtained. During the adsorption process we consider two main components, i.e., adsorbent and adsorbate. *Adsorbent* is a solid on which the adsorption process occurs. Usually it is a very porous material which contains the high specific surface area. Different types of adsorbents (depending on the adsorbate) are used: natural adsorbents (e.g., biochar, clay minerals or clay based adsorbents, fly ash, wood) or engineered adsorbents (e.g., silica gels, activated carbons). *Adsorbate* is the material which is adsorbed (mainly organic or non-organic pollutants, such as industrial effluents, oils or heavy metals). Depending on the adsorbate various adsorbents may be used: for example, for air cleaning at home the activated carbon filters are used, for removing moisture silica gel granules are used.

Various aspects of the adsorption process are analyzed and discussed [12,17]. Different adsorption models are reported, analyzed and applied to the experimental data with different adsorbents [7, 8, 10, 13]. Some of the models are based on adsorption reaction models and the adsorption kinetics is represented as the rate of chemical reactions. Other authors investigate the influence of the model parameters (mass transfer coefficient, surface diffusion or pore diffusivity) [9, 11]. Less works are dedicated to the direct numerical simulation of reactive flow when the scientists should choose the appropriate solute transport model [7]. In general case, mathematical models can be classified as given in [13]: (i) adsorption reaction models; (ii) adsorption diffusion models; and (iii) pore volume and surface diffusion models. The models with mass transfer diffusion are more complicated, but these models are most realistic. Some authors analyzed and compared the adsorption results obtained using different diffusion models [11, 16]. We note, that in this case the system of partial differential equations (PDEs) with appropriate boundary conditions is nonlinear and quite complicated. Thus numerical methods are used for solving such problems. For approximation of the system of PDEs different numerical methods are applied. In [8] the conservative averaging method was used. In [7], the finite volume method is applied to approximate the system of PDE. For solving adsorption problems a various computational software was used. For example in [7] calculations were performed by combining the special commercial software package (GeoDict) and a general non-commercial software (Pore-Chem). The results of [8, 13] were obtained by using MATLAB software. In [11] the program PDESOL was applied.

In this paper we consider the complex pore volume and surface diffusion model, presented also in [11, 13, 16]. This model includes bulk liquid phase mass balance and the mass balance equation for both solid and liquid phases of the particle. We consider the special methods for appropriate numerical approximation of the model for adsorption kinetics, analyze the stability of the obtained discrete problem and investigate the sensitivity of the solution with

respect of main transport and kinetic parameters. On the basis of this analysis it is shown how the adsorption process can be controlled efficiently. The obtained results make a basis for solving some important applied optimization problems– to maximize the amount of adsorbate by selecting the optimal shape parameter of the adsorbent.

The paper is organized as follows. In Section 2 we describe the mathematical adsorption model for the liquid-solid system. The approximation of the obtained system of nonlinear PDEs is done in Section 3. The application of standard adaptive ODE solvers and the analysis of different methods to construct adaptive in time discrete meshes are done in Section 4. The analysis of adaptive integrators for ODEs simulating parabolic problems is done in Section 5. The main goal is to control the global error of the discrete solution in the maximum norm, i.e. not restricting to the final time of the simulation. In Section 6 a more detailed analysis of ODE solvers is presented for the ODE system describing the surface kinetics. In order to understand and to control effectively the adsorption process we propose and analyze the linearized adsorption kinetics model. Using this model we can predict the dynamics of the adsorption process. The results are presented in Section 7. It shown that using such simplification we can model the adsorption process quite accurately. Results of numerical experiments (for the full and linearized models) are presented and discussed in Section 7. It is shown that using the proposed simplified linear models we can predict the main trend of the adsorption process quite accurately.

2 The mathematical model of the liquid-solid adsorption kinetics

In this section we present the liquid-solid adsorption kinetics model also used in [11, 13, 16]. It is important to note that we consider all main physical processes, including kinetics and the pore volume and surface diffusion. The following assumptions are used [13]: the system is isothermal, all particles are spherical and of the same size, there exists adsorption equilibrium between the pore and the average porosity and tortuosity of the particle. The model takes into account three concentrations: the bulk liquid concentration (C_B), the concentration of the solute in the liquid (C_L) and the concentration in the solid (C_S). In the particle we consider two processes: the solute diffusion from the particle surface to the center of the particle and the adsorption equilibrium in the particle represented by an isotherm. The surface diffusion occurs due interactions between the solute and the solid.

On the surface of the particle the solute flux from the bulk to the liquid phase is proportional to the difference between the bulk concentration and the concentration of the liquid solute on the surface of the particle. This process is described by (2.1) equation:

$$\frac{\partial C_B(t)}{\partial t} = -k_m A\Big(C_B(t) - C_L(t,r)\big|_{r=R_p}\Big), \tag{2.1}$$

here k_m is the external mass transfer coefficient, $A = \frac{mS}{V}$, m is the mass of

adsorbent, S is the external surface area per mass of adsorbent, V is the volume of solution, R_p is the particle radius.

Next we describe the mass balance in the particle. The combined transport in two phases is considered. According to the Fick low the overall transport flux is a sum of void and adsorbate phase transport fluxes [14]

$$J = \varepsilon J_P + (1-\varepsilon) J_S,$$

where $J_P = -D_P \frac{\partial C_L}{\partial r}$ is the diffusion flux from the particle surface to the center of the pores and $J_S = -D_S^0 \frac{\partial C_S}{\partial r}$ defines the diffusion flux on the solid surface. Assuming the local equilibrium for chemical potential between the adsorbed phase (solid) and not adsorbed phase (liquid) J_S can be written as [14]:

$$J_S = -LC_S \frac{\partial \mu_S}{\partial r}, \quad \mu_S = \mu_L = \mu_0 + RT \ln(C_L),$$

where R is the ideal gas constant, L is the mobility constant and T is temperature. Then the flux can be expressed as

$$J_S = -D_S \frac{C_S}{C_L} \frac{\partial C_L}{\partial C_S} \frac{\partial C_S}{\partial r},$$

where $D_S = RLT$. As a result we get the overall mass balance equation

$$\begin{aligned} &\varepsilon \frac{\partial C_L(t,r)}{\partial t} + (1-\varepsilon) \frac{\partial C_S(t,r)}{\partial t} \\ &\quad = \frac{1}{r^2} \frac{\partial}{\partial r} \left(\varepsilon D_P r^2 \frac{\partial C_L(t,r)}{\partial r} + (1-\varepsilon) D_S r^2 \frac{C_S(t,r)}{C_L(t,r)} \frac{\partial C_L(t,r)}{\partial r} \right), \end{aligned} \tag{2.2}$$

where ε is the particle porosity, r is the particle radial direction, D_P is the pore diffusivity and D_S is the surface diffusivity. As it is shown in [7,13,14] the surface diffusion depends on the used isotherm for the equilibrium conditions. As an example, let us consider the Langmuir isotherm

$$C_S(t,r) = C_{S,*} b \frac{C_L(t,r)}{1 + bC_L(t,r)}, \tag{2.3}$$

where b is a Langmuir adsorption constant and $C_{S,*}$ is the saturation solute solid concentration. Then equation (2.4) represents the overall mass balance in the particle: through the liquid phase concentration

$$\begin{aligned} &\left(\varepsilon + (1-\varepsilon) \frac{\partial C_S}{\partial C_L} \right) \frac{\partial C_L(t,r)}{\partial t} \\ &\quad = \frac{1}{r^2} \frac{\partial}{\partial r} \left(r^2 \left(\varepsilon D_P + (1-\varepsilon) D_S \frac{C_{S,*} b}{1 + bC_L(t,r)} \right) \frac{\partial C_L(t,r)}{\partial r} \right). \end{aligned} \tag{2.4}$$

This system of ODE (2.1) and PDE (2.2) is supplemented with initial and boundary conditions:

$$C_B(0) = C_B^0, \quad C_L(0,r) = C_L^0, \ \ 0 \le r \le R_p, \tag{2.5}$$

$$r^2 \frac{\partial C_L(t,r)}{\partial r}\Big|_{r=0} = 0, \quad r^2 \frac{\partial C_S(t,r)}{\partial r}\Big|_{r=0} = 0, \tag{2.6}$$

$$\Big(\varepsilon D_P + (1-\varepsilon) D_S \frac{C_S(t,r)}{C_L(t,r)}\Big) \frac{\partial C_L(t,r)}{\partial r}\Big|_{r=R_p} = k_m\big(C_B(t) - C_L(t,r)\big|_{r=R_p}\big), \tag{2.7}$$

where k_m is the mass transfer coefficient.

The initial conditions (2.5) represent the bulk concentration and solute concentration in the liquid phase inside the particle at the initial time moment. Equations (2.6) define the symmetry conditions for C_S and C_L concentrations at the center of the particle. As the boundary condition for $r = R_p$ the continuity condition (2.7) on the surface of the particle is used. In the case of the Langmuir isotherm (2.3) this boundary condition is defined as:

$$\Big(\varepsilon D_P + (1-\varepsilon) D_S \frac{C_{S,*} b}{1 + bC_L(t,r)}\Big) \frac{\partial C_L(t,r)}{\partial r}\Big|_{r=R_p} = k_m\big(C_B(t) - C_L(t,r)\big|_{r=R_p}\big). \tag{2.8}$$

In [7] it is shown that the choice of correct isotherm is a very important part of the model selection. The adsorption isotherm represents the relationship between the adsorbate concentration in the solid and in the liquid. The adsorption equilibrium conditions imply the dynamics of the full process. The required isotherms should be chosen by taking into account properties of the solute, the order of the reaction and the interface type [7].

A number of different isotherms are described in literature. The most frequently used isotherms are [2, 7, 14]: a) the Henry isotherm $C_S = KC_L$, b) the Langmuir isotherm $C_S = C_{S,*} bC_L/(1 + bC_L)$, c) the Freundlich isotherm $C_S = K_F C_L^{1/n}$, d) the Redlich–Peterson $C_S = k_{RP} C_L/(1 + a_{RP} C_L^{\beta})$, e) the Sips isotherm $C_S = C_{S,*}(bC_L)^{1/n}/(1 + (bC_L)^{1/n})$.

3 Approximation of the model

The approximation of the mathematical model (2.1)–(2.7) is done by using the method of lines. First, the semi-discrete finite volume scheme is constructed to approximate in space the nonlinear PDE (2.2). In order to simplify notations we restrict to the Langmuir adsorption model (2.3).

The uniform spatial mesh $\bar{\omega}_h = \omega \cup \{r_J\}$ is defined as

$$\omega_h = \{r_j : \ r_j = (j - 1/2)h, \ \ j = 1, \dots, J-1\}, \quad r_J = R_p, \ h = R_p/(J - 0.5).$$

Multiplying equation (2.3) by r^2, integrating it over finite volume $[r_{j-0.5}, r_{j+0.5}]$ and approximating the obtained fluxes by central difference formula we obtain the semi-discrete scheme for $j = 1, ..., J-1$

$$\frac{r_{j+1/2}^3 - r_{j-1/2}^3}{3} \left(\varepsilon + (1-\varepsilon) \frac{bC_{S,*}}{(1 + bC_{L,j})^2}\right) \frac{\partial C_{L,j}(t)}{\partial t}$$

$$= r_{j+1/2}^2 \left(\varepsilon D_P + (1-\varepsilon) D_S \frac{bC_{S,*}}{1+0.5b(C_{L,j+1}+C_{L,j})} \right) \frac{C_{L,j+1}-C_{L,j}}{h}$$
$$- r_{j-1/2}^2 \left(\varepsilon D_P + (1-\varepsilon) D_S \frac{bC_{S,*}}{1+0.5b(C_{L,j}+C_{L,j-1})} \right) \frac{C_{L,j}-C_{L,j-1}}{h}.$$

Boundary conditions are approximated in a similar way. For example, the condition (2.8) is approximated by the semi-discrete equation (3.1)

$$\frac{h}{2} r_J^2 \left(\varepsilon + (1-\varepsilon) \frac{bC_{S,*}}{(1+bC_{L,J})^2} \right) \frac{\partial C_{L,J}(t)}{\partial t} = -r_{J-1/2}^2 \Big(\varepsilon D_p + (1-\varepsilon) D_S$$
$$\times \frac{bC_{S,*}}{1+0.5b(C_{L,J}+C_{L,J-1})} \Big) \frac{C_{L,J}-C_{L,J-1}}{h} + r_J^2 k_m (C_B(t) - C_{L,J}). \quad (3.1)$$

The proposed finite volume scheme approximates the given nonlinear differential problem with the second order accuracy. Due to properties of nonlinear coefficients it is straightforward to show that for implicit approximations of the time derivatives the fully discrete scheme is also unconditionally stable and the discrete solution converges to the exact solution of the differential problem. In this case the known theoretical results [4, 6] can be applied to prove that the solution of the semi- discrete scheme converges in the L_∞ norm with the order equal to the accuracy of approximation.

By adding the mass balance equation for the bulk concentration C_B

$$\frac{\partial C_B(t)}{\partial t} = -k_m A (C_B(t) - C_{L,J}(t))$$

we obtain a large system of nonlinear ODEs with respect to functions $C_{L,j}(t)$, $j = 1, \ldots, J$ and $C_B(t)$.

For some sets of coefficients this system of ODEs defines a very stiff problem, thus appropriate solvers should be used to solve it. In our computational experiments we use the MATLAB ode15s solver. The analysis of some general adaptive solvers for stiff ODEs is presented in the next section.

4 Adaptive ODE solvers

It is well-known that two main challenges should be solved when stiff ODE systems are integrated. First, the unconditional stability of the numerical algorithm should be guaranteed. Second, the scheme should have the ability to produce time grids on which the main features of the solution are sufficiently resolved [1].

We start our analysis with a simple model ODE problem

$$\frac{du}{dt} = \lambda u, \quad u(0) = u_0, \quad t \in [0, T], \ \lambda > 0. \quad (4.1)$$

It describes the case of a linear source function and the solution is defined as

$$u(t) = u_0 e^{\lambda t}. \quad (4.2)$$

We note, that for problems when the eigenvalues of the discrete operator have positive real parts and the problem is non-stiff, explicit integration algorithms can be used (e.g. the forward Euler scheme). But for stiff problems the unconditional stability requirement leads to application of implicit solvers. As the first example of discrete integrator we consider the implicit backward Euler scheme and approximate the problem (4.1) as:

$$\frac{U^n - U^{n-1}}{\tau_n} = \lambda U^n, \quad n = 1, \dots, N, \tag{4.3}$$

where the nonuniform time mesh is defined as $t_n = t_{n-1} + \tau_n$, $t_0 = 0$. Here U^n is the discrete solution which approximates the exact solution $u(t_n)$.

The local truncation error at $t = t_n$ is defined by

$$\psi^n = \frac{u(t_n) - u(t_{n-1})}{\tau_n} - \lambda u(t_n).$$

It can be bounded like

$$|\psi^n| \leqslant \frac{\tau_n}{2} |u''(t_n)|. \tag{4.4}$$

Next we consider the error $Z^n = U^n - u(t_n)$. Substituting $U^n = Z^n + u(t_n)$ into (4.3) we obtain the same discrete equation as (4.3) but with the right-hand side ψ^n:

$$\frac{Z^n - Z^{n-1}}{\tau_n} = \lambda Z^n - \psi^n.$$

Then we have that

$$Z^n = \frac{1}{1 - \tau_n \lambda} (Z^{n-1} - \tau_n \psi^n)$$

from which the standard stability estimate follows

$$|Z^n| \leqslant \rho_n (|Z^{n-1}| + \tau_n |\psi^n|), \quad \rho_n = \frac{1}{|1 - \tau_n \lambda|}. \tag{4.5}$$

Application of (4.5) recursively and the initial condition $Z^0 = 0$ yields the a priori error estimate

$$|Z^n| \leqslant \sum_{k=1}^{n} (\prod_{l=k}^{n} \rho_l) |\psi^k| \tau_k. \tag{4.6}$$

If the explicit Euler method is used to integrate the problem (4.1)

$$\frac{U^n - U^{n-1}}{\tau_n} = \lambda U^{n-1}, \; t_n = t_{n-1} + \tau_n, \; t_0 = 0, \tag{4.7}$$

then the same error estimate (4.6) is valid, only the stability factor ρ_n is defined as

$$\rho_n = 1 + \tau \lambda_n.$$

Different step-size control algorithms can be derived from (4.6). Assuming the step size τ_n to be sufficiently small, the stability factor ρ_n can be estimated as $\rho_n \approx \mathrm{e}^{\lambda \tau_n}$. Then we get that

$$\prod_{l=k}^{n} \rho_l = \mathrm{e}^{\lambda (t_n - t_{k-1})}.$$

It follows from the estimate of the truncation error (4.4), the explicit form of the exact solution (4.2) and the stability inequality (4.6), that the first step-size control can be based on the global (uniform) a priori error estimate

$$|Z^n| \leqslant 0.5\lambda^2 u_0 \sum_{k=1}^{n} (\prod_{l=k}^{n} \rho_l) e^{\lambda t_k} (\tau_k)^2 \leqslant 0.5\lambda^2 u_0 t_n e^{\lambda t_n} \max_{1\leqslant k\leqslant n} |\tau_k|.$$

Lemma 1. *In order to guarantee the estimate $|Z^n| \leqslant \varepsilon$ it is sufficient to use the uniform time mesh with the time-step size:*

$$\tau_k = 2\varepsilon/(\lambda^2 u_0 t_n e^{\lambda t_n}), \quad k = 1, \dots, n.$$

It is clear, that such a uniform mesh is sufficient to solve the given problem with the required accuracy. A more challenging task is to find the optimal distribution of mesh points. Different objective functions can be considered.

Lemma 2. *The time mesh obtained by minimizing the global error Z^n for a given number of grid points is uniform with time step sizes*

$$\Big(\prod_{l=k}^{n} \rho_l\Big) |\psi^k| \tau_k = c, \quad k = 1, \dots, n. \tag{4.8}$$

Here $|\psi^k|\tau_k$ defines the local error accumulated on the element $[t_{k-1}, t_k]$ and $w_k = \prod_{l=k}^{n} \rho_l$ are the weights.

The proof follows directly from results of [1, 5]. A standard and more general way to compute the weights is to solve a dual problem to the given discrete problem.

It is interesting to note, that for the given test problem the optimal mesh is uniform. The same conclusion is valid also in the case of parabolic type problems, when $\lambda < 0$. This conclusion is quite counter-intuitive, since it is natural to expect that for an adaptive time mesh smaller step-sizes should be taken to resolve faster changes of the solution.

The popular MATLAB solver ode15s, which is targeted to solve stiff ODEs, applies *hp*-adaptivity, i.e. the algorithm selects the approximation order and adaptive time step size. The numerical integrators are defined by the backward difference formula (BDF) or by the numerical differentiation formula (NDF) [3]. For the adaptive step size control the approximate local truncation error

$$LTE = C\tau_n^{k+1} \|U^{k+1}(t_n)\| \tag{4.9}$$

is used. Here k is the order of the selected BDF or NDF algorithm. It follows from the analysis given above that this monitoring function is similar to the optimal step size control estimate (4.8), only the weights w_k are simplified and some a priori constant C is used.

5 A control of the error in the maximum norm

In the previous section we derived the optimal time grid when the error is controlled only at the final time moment. This objective function is well fitted if the solution is a growing function and the error at the final time moment is reaching the maximal value. Now we consider the model problem

$$\frac{du}{dt} + \lambda u = 0, \quad u(0) = u_0, \quad t \in [0, T], \ \lambda > 0. \tag{5.1}$$

It simulates the simplified diffusion equation and the solution is defined as

$$u(t) = u_0 e^{-\lambda t}.$$

Again we solve the model problem by using the backward Euler method

$$\frac{U^n - U^{n-1}}{\tau_n} + \lambda U^n = 0, \ t_n = t_{n-1} + \tau_n, \ t_0 = 0. \tag{5.2}$$

The error at the time moment $t = t_n$ satisfies the equation

$$Z^n = \frac{1}{1 + \tau_n \lambda}(Z^{n-1} - \tau_n \psi^n). \tag{5.3}$$

Repeating the analysis of the previous section we get the estimate

$$|Z^n| \leqslant \sum_{k=0}^{n-1} \tau \rho^{k+1} |\psi^{n-k}| \leqslant \frac{\tau}{2} \lambda^2 t_n \mathrm{e}^{-\lambda t_n} u_0, \tag{5.4}$$

where the stability factor is defined as $\rho_n = 1/(1 + \tau_n \lambda)$. It follows from (5.4) that the error bound has the maximum value at $t^m = 1/\lambda$ and thus we can rewrite the error estimate in the form

$$|Z^n| \leqslant \frac{\tau}{2} \lambda \mathrm{e}^{-1} u_0, \quad n = 1, \ldots, m.$$

Now let us solve this problem with accuracy ε in the interval $[0, T]$. It follows from the analysis of equation (4.1) that for the backward Euler scheme in the time interval $[0, 1/\lambda]$ the optimal time mesh is uniform with the time step size

$$\tau_0 \leqslant 2\mathrm{e}\varepsilon/(\lambda u_0).$$

Now we make the important conclusion from the stability estimate (5.3). In order to guarantee the same accuracy of the discrete solution for all $t \in [1/\lambda, T]$, it is possible to increase dynamically the sizes of time steps and to reduce the total computation complexity of the integration algorithm. According to (5.3) the time step size τ_n can be computed from the equality

$$\varepsilon = \frac{1}{1 + \tau_n \lambda}(\varepsilon + \tau_n |\psi^n|).$$

Taking into account that $\psi^n = 0.5 \tau_n \lambda^2 u_0 \exp(-\lambda t_{n-1})$, for $t_n = t_{n-1} + \tau_n$, $t_n > t^m$ and $\exp(-\lambda t^m) = 1/e$, we define the time step size of the adaptive mesh:

$$\tau_n = \frac{2\varepsilon e^{\lambda t_{n-1}}}{\lambda u_0} = \tau_0 e^{\lambda(t_{n-1} - t^m)}.$$

Thus we have proved the following result.

Lemma 3. *For the parabolic model problem* (5.1) *the error of the discrete solution of the backward Euler scheme* (5.2) *is uniformly less than the specified accuracy constant* ε *if the following adaptive mesh is used*

$$\tau_n = 2e\varepsilon/(\lambda u_0), \quad \textit{for } t_n \leqslant t^m,$$
$$\tau_n = \tau_0 e^{\lambda(t_{n-1}-t^m)}, \quad \textit{for } t^m < t_n \leqslant T.$$

The proposed dynamics of the adaptive time step sizes is qualitatively similar to adaptive grids generated by using MATLAB type error monitors (4.9). Still for the latter solver the time step sizes are changing in a more moderate way

$$\tau_n = \widetilde{\tau}_0 \mathrm{e}^{0.5\lambda t_{n-1}}.$$

We will mention one interesting relation between forward and backward Euler schemes. It is easy to see, that the explicit forward Euler scheme (4.7) can be considered as the implicit backward Euler scheme, only moving backward in t:

$$\frac{U^{n-1} - U^n}{\tau_n} + \lambda U^{n-1} = 0, \; t_{n-1} = t_n - \tau_n, \; t_N = T.$$

Thus the solutions U^n of the explicit forward Euler scheme (4.7) are poor approximations of the growing exact solution of the problem (4.1), however they are good approximations to the solution of the problem

$$\frac{d\widetilde{u}}{dt} = \lambda \widetilde{u}, \quad \widetilde{u}(T) = U^N, \quad t \in [0, T], \; \lambda > 0.$$

Thus the solution U^n shadows a solution of the same differential problem but with a different ("wrong") initial condition. The shadowing phenomena is well-explained in the expository paper [15], see also references given therein.

6 Integration of the surface kinetics equations

In this section we analyze the system of differential equations

$$\begin{cases} \dfrac{du}{dt} = \alpha(v - u), \quad u(0) = 1, \\ \dfrac{dv}{dt} + \gamma v = \beta(u - v), \quad v(0) = 0. \end{cases} \tag{6.1}$$

The given test problem describes a simplified model for surface adsorption kinetics. The linear sink term γv simulates the diffusion processes. If coefficients $\alpha, \beta \gg 1$ are large and $\gamma = 0$ (no diffusion), then the solution fastly reaches the stationary value

$$u^* = v^* = \beta/(\alpha + \beta).$$

If $\gamma > 0$, the the adsorption kinetics is described by two stages: first a quasi-stationary solution is fastly reached and then both components decay slowly due to the linear sink term.

Next we present some results of computational experiments. The following values of parameters are used: $\alpha = 10, 100$, $\beta = 2\alpha$, $\gamma = 0, 1$ and the time

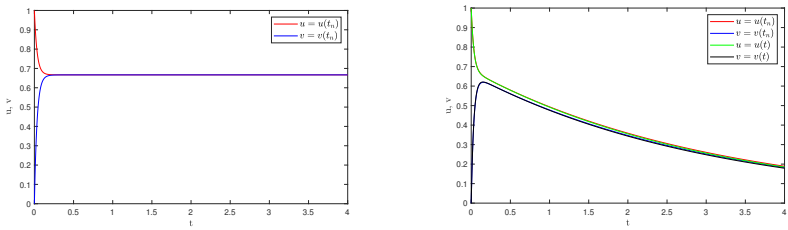

a) b)

Figure 1. Solutions of the initial value problem (6.1): a) $\gamma = 0$, b) $\gamma = 1$.

interval $[0, 4]$. In Figure 1 the solutions of problem (6.1) are shown for different values of γ.

Figure 2 represents the sizes of time steps selected by ODE15s solver when the approximation order was reduced to one (the backward Euler method). The system is solved in the time interval $[0, 4]$ with different values of the parameters α, β and γ.

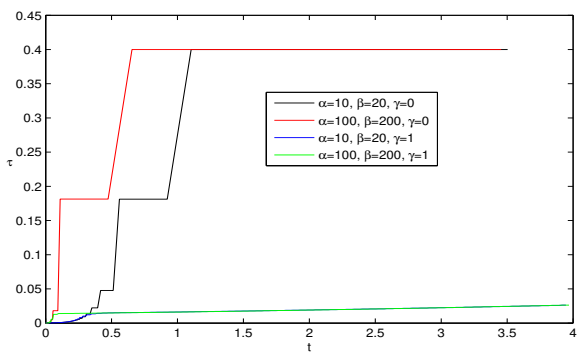

Figure 2. Time steps in time interval $[0, 4]$ with different values of the parameters.

We see that in the case $\gamma = 0$ the solution reaches the equilibrium state very fast (depending on the values of α and β) and the integration step size also fastly increases till the maximal allowed step. But in the case of $\gamma = 1$ due to the slow sink process the time step is adapted to resolve the dynamics of the solution and it increases not so fast as in the case of $\gamma = 0$.

7 The sensitivity analysis of the simplified adsorption kinetics model

In this section we introduce the simplified adsorption kinetics model with initial and boundary conditions:

$$\frac{\partial C_B(\bar{t})}{\partial \bar{t}} = -\alpha(C_B(\bar{t}) - C_L(\bar{t},1)), \quad 0 < t < \bar{T}, \tag{7.1}$$

$$\frac{\partial C_L(\bar{t},\bar{r})}{\partial \bar{t}} = \frac{1}{\bar{r}^2}\frac{\partial}{\partial \bar{r}}\left(\bar{r}^2\frac{\partial C_L(\bar{t},\bar{r})}{\partial \bar{r}}\right), \quad 0 < \bar{r} < 1, \tag{7.2}$$

$$\bar{r}^2\frac{\partial C_L(\bar{t},\bar{r})}{\partial \bar{r}}\Big|_{\bar{r}=0} = 0, \quad \frac{\partial C_L(\bar{t},\bar{r})}{\partial \bar{r}}\Big|_{\bar{r}=1} = \beta(C_B(\bar{t}) - C_L(\bar{t},1)), \tag{7.3}$$

$$C_B(0) = C_B^0, \quad C_L(0,\bar{r}) = C_L^0, \ \ 0 \leqslant \bar{r} \leqslant 1. \tag{7.4}$$

These equations are obtained from (2.1), (2.2), (2.5)–(2.7) using dimensionless variables

$$r = R_p\bar{r}, \ \ t = \frac{cR_p^2}{D}\bar{t}, \ \ 0 < \bar{r} < 1, \ \ 0 < \bar{t} < \bar{T} = \frac{TD}{cR_p^2}$$

and linearizing nonlinear equation on the equilibrium isotherm

$$C_S(\bar{t},\bar{r}) = f(C_L(\bar{t},\bar{r}))$$

with $c = \varepsilon + (1-\varepsilon)f'(C_L)$. The combined diffusion coefficient is selected as

$$D = \varepsilon D_p + (1-\varepsilon)D_s\frac{f(C_L)}{C_L}.$$

New mass transport parameters α and β are computed as:

$$\alpha = \frac{Ak_m cR_p^2}{D}, \quad \beta = \frac{k_m R_p}{D}. \tag{7.5}$$

We use the linearized and normalized mathematical model (7.1)–(7.4) for the sensitivity analysis with respect to the parameters of adsorption system.

We test the simplified model on the data reported by V. Russo et al. [13] and P. R. Souza et al. [16]. In [13] the Langmuir isotherm for the equilibrium was used. For the set of parameters reported in [13] we solve the full adsorption kinetics model first. In Figure 3 we see the change of the bulk concentration ($C_B(t)$) and the change of the concentration of the solute in the liquid on the surface of the particle ($C_L(t,R_p)$) and at the center of the particle ($C_L(t,0)$) along the time. We see that the bulk concentration reaches the saturation very fast. This is determined by the boundary condition: the change in the bulk concentration causes the change of the concentration of the solute in the liquid phase on the surface of the particle. But still we have a slow transport (diffusion) process inside of the particle. Therefore the concentration of the solute in the liquid at the center of the particle changes very slowly along the time.

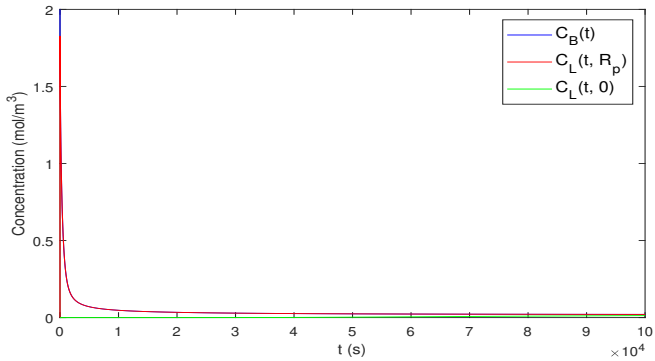

Figure 3. Bulk concentration, concentration of the solute in the liquid on the surface of the particle and concentration of the solute in the liquid at the center of the particle for the data reported in [13].

The second example illustrates an opposite situation when the concentration of the solute in the liquid at the center of the particle changes much faster and it reaches equilibrium state only shortly after surface concentration (Figure 4). In this case we use the data reported in [16] with the Redlich-Peterson isotherm. Some model parameters are estimated or converted using the provided data in order to compare the change of the concentrations for the two analyzed problems.

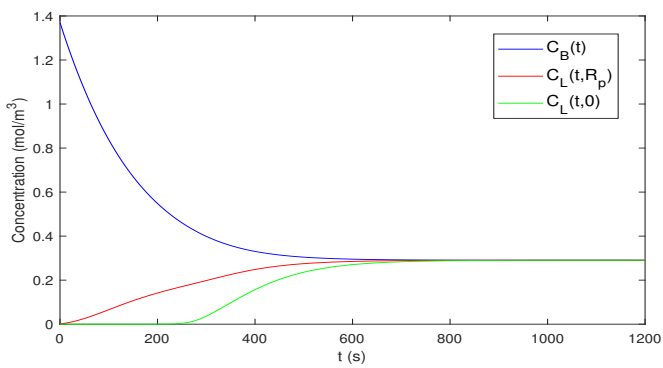

Figure 4. Bulk concentration, concentration of the solute in the liquid on the surface of the particle and concentration of the solute in the liquid at the center of the particle for the data reported in [16].

We find that these two examples illustrate different properties of the adsorption process. In the presented figures we observe qualitatively different results. We remind that the full mathematical model is used in the analysis given above.

Next we use the linearized and normalized mathematical model to the discussed problems and concentrate on the dynamics of the bulk concentration

$(C_B(\bar{t}))$, concentration of the solute in the liquid on the surface of the particle $(C_L(\bar{t}, 1))$ and concentration of the solute in the liquid at the center of the particle $(C_L(\bar{t}, 0))$. The Figures 5 and 6 show that with the simplified model we can predict the dynamics of the process quite accurately.

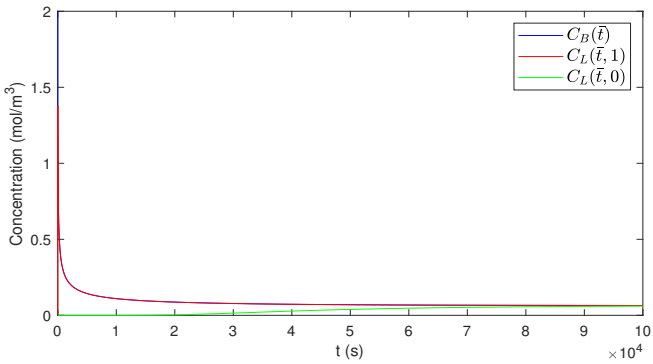

Figure 5. Dynamics of the concentrations obtained from the simplified model for the data reported in [13].

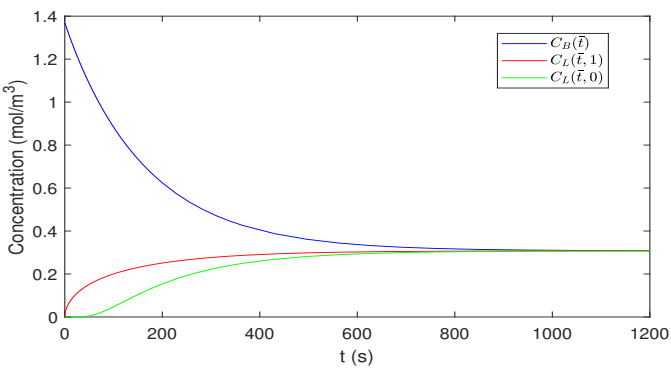

Figure 6. Dynamics of the concentrations obtained from the simplified model for the data reported in [16].

Now we focus on the sensitivity analysis. In order to investigate the influence of physical parameters on solutions, we performed a detailed analysis of the second example based on data provided in [16]. With this set of parameters we find that the simplified model parameters are $\alpha = 4.14$ and $\beta = 0.4$. We see that the parameter α controls the decay of the bulk concentration. The higher is the value of this parameter the faster bulk concentration $C_B(\bar{t})$ decreases and the process reaches the equilibrium with the lower concentration (see Figure 7). The concentration on the surface of the particle $C_L(\bar{t}, 1)$ does not increases so fast.

The parameter β affects the change in concentration on the surface of the

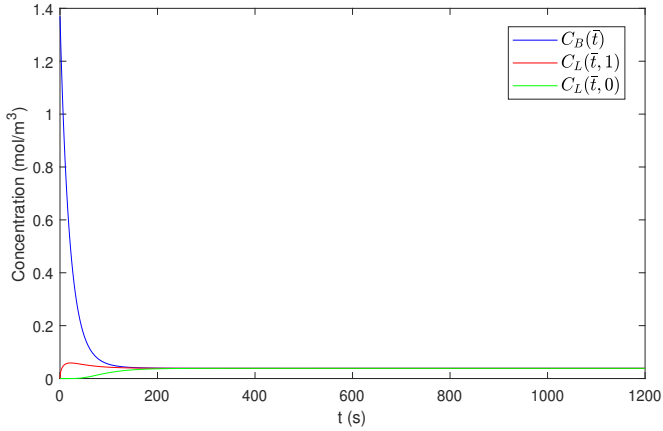

Figure 7. Dynamics of the concentrations obtained from the simplified model ($\alpha = 41.4$, $\beta = 0.4$) for the data reported in [16].

particle: the higher the value of this parameter the faster concentration $C_L(\bar{t}, 1)$ increases (Figure 8).

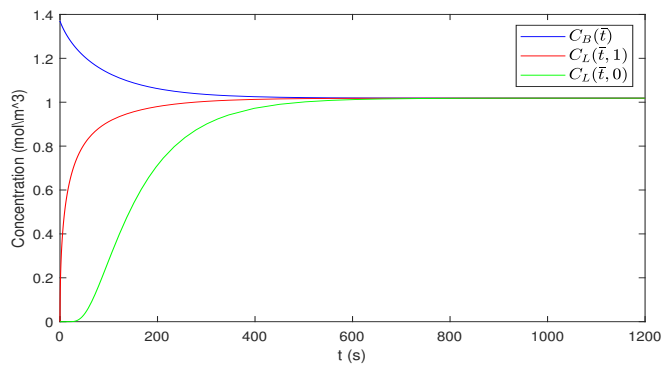

Figure 8. Dynamics of the concentrations obtained from the simplified model ($\alpha = 4.14$, $\beta = 4$) for the data reported in [16].

As it was shown in Section 6 the adsorption kinetics depends not only on the absolute values of parameters, but also on their ratio. We see the influence of the ratio α/β in Figure 8 ($\alpha/\beta \approx 1$), Figure 9 ($\alpha/\beta \approx 10$) and Figure 10 ($\alpha/\beta \approx 0.1$). We conclude that the ratio of parameters influences the equilibrium concentration and the time required to reach this concentration. If α/β is large then the system fast reaches equilibrium with lower the bulk concentration. In the case when $\alpha/\beta \ll 1$ the system reaches equilibrium with high bulk concentration and needs more time.

Now we analyze which physical parameters influence such changes. From the (7.5) we find that $\alpha/\beta = AcR_p$. This means that the adsorption process

depends on the properties of the adsorbent and solution, on the isotherm used for equilibrium and the radius of the particle. In Figure 11 we present the concentrations obtained using Langmuir isotherm estimated from the data reported in [16]. The results show that in our case when isotherms fit quite well to the given data we can observe the same adsorption process development (see Figure 6 for comparison).

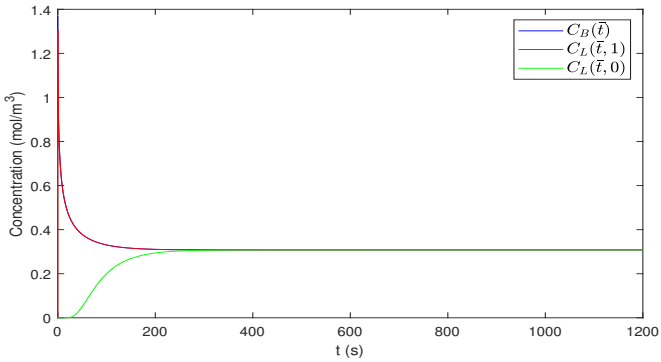

Figure 9. Dynamics of the concentrations obtained from the simplified model ($\alpha/\beta \approx 10$) for the data reported in [16].

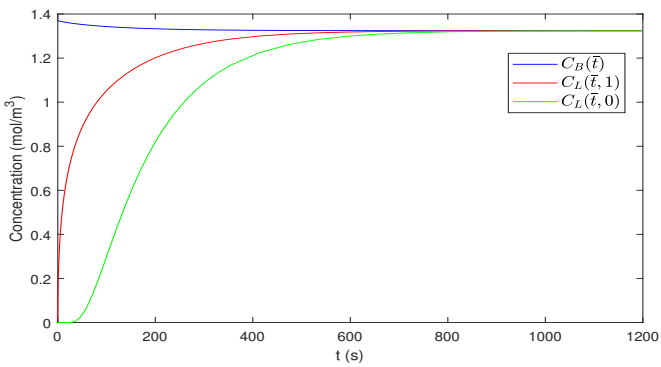

Figure 10. Dynamics of the concentrations obtained from the simplified model ($\alpha/\beta \approx 0.1$) for the data reported in [16].

After performed simulations we see that the linearized and normalized mathematical model works well and we can predict the dynamics of the process with a different set of physical parameters quite accurately. As we see from calculations with a full adsorption model the bulk concentration decreases for both examples (see Figure 3 and Figure 4), but for the first example the process is faster. Let us compare the results obtained using the full and the simplified models for the data reported in [13]. In this case the full model (see Figure 3) shows that the bulk concentration decreases very fast and the pore concentration of the solute in the liquid increases till a saturation is reached. During a

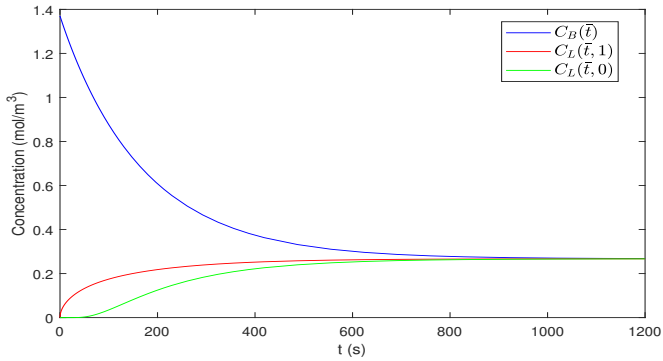

Figure 11. Dynamics of the concentrations obtained from the simplified model with Langmuir isotherm for the data reported in [16].

short time interval (depending on the physical parameters) the concentration of solute in the liquid at the surface of the particle increases very fast and a quasi-stationary solution is fastly reached. Then both solutions decay together. The change of the concentration on the surface of the particle implies the change of the concentration in the pore. This process is very slow for this example. And the pore is fully filled only after a long time interval. As we can see the saturation at the center of the particle even after 100 000 s is still not reached.

Analogous information is obtained from the simplified model (see Figure 5). Using this model we find that the concentration of solute in the liquid at the surface of the particle increases very fast and reaches the value of bulk concentration. The change in the concentration inside the particle is a slow process and needs time to reach the center of the particle. We should note that the quasistationary concentration and the rate of adsorption process differ from the full model solutions. Such differences can be explained by the influence of the parameters c and D used in simplified model. The values of these parameters do not change according to time in the simplified model and such simplification implies the quantitative changes in solutions. But we model the main trend of the adsorption process quite accurately.

8 Conclusions

The pore volume and the surface diffusion model for the liquid-solid adsorption is considered. The numerical methods for the adsorption kinetics model are constructed, the stability analysis for the discrete problem and the global error control are discussed.

The sensitivity of the solution with respect of main physical system parameters is analyzed using the simplified model. This analysis allows to predict the dynamics of the adsorption process. The results obtained with the linearized and normalized mathematical model are compared with the simulations done for a full nonlinear mathematical model. The results of the numerical experiments show that we can predict the main trend of the adsorption process using

the proposed simplified linear model.

The obtained results can be applied for optimization problems.

Acknowledgements

The authors of this research Edita Baltrėnaitė and Teresė Leonavičienė were partially supported by the Research Council of Lithuania (project No. S-MIP-17-83).

References

[1] W. Bangerth and R. Rannacher. *Adaptive Finite Element Methods for Solving Differential Equations*. Birkhäuser, Basel, 2003. https://doi.org/10.1007/978-3-0348-7605-6.

[2] M. Belhachemi and F. Addoun. Comparative adsorption isotherms and modeling of methylene blue onto activated carbons. *Applied Water Science*, **1**(3–4):111–117, 2011. https://doi.org/10.1007/s13201-011-0014-1.

[3] E. Alberdi Celaya, J.J. Anza Aguirrezabala and P. Chatzipantelidis. Implementation of adaptive bdf2 formula and comparison with the matlab ode15s. *Procedia Computer Science*, **29**:1014–1026, 2014. https://doi.org/10.1016/j.procs.2014.05.091.

[4] R. Čiegis and N. Tumanova. Numerical solution of parabolic problems with nonlocal boundary conditions. *Numerical Functional Analysis and Optimization*, **31**(12):1318–1329, 2010. https://doi.org/10.1080/01630563.2010.526734.

[5] K. Eriksson, D. Estep, P. Hansbo and C. Johnson. *Computational Differential Equations*. Cambridge University Press, 1996.

[6] W. Hundsdorfer and J.G. Verwer. *Numerical Solution of Time-Dependent Advection-Difusion-Reaction Equations*. Springer Series in Computational Mathematics, 33. Springer, Berlin, Heidelberg, New York, Tokyo, 2003.

[7] O. Iliev, Z. Lakdawala, K.H.L. Neßler, T. Prill, Y. Vutov, Y. Yang and J. Yao. On the pore-scale modeling and simulation of reactive transport in 3d geometries. *Mathematical Modelling and Analysis*, **22**(5):671–694, 2017. https://doi.org/10.3846/13926292.2017.1356759.

[8] I. Kangro and H. Kalis. On mathematical modelling of the solid-liquid mixtures transport in porous axial-symmetrical container with Henry and Langmuir sorption kinetics. *Mathematical Modelling and Analysis*, **23**(4):554–567, 2018. https://doi.org/10.3846/mma.2018.033.

[9] M. Kavand, N. Asasian, M. Soleimani, T. Kaghazchi and R. Bardestani. Film-pore-[concentration-dependent] surface diffusion model for heavy metal ions adsorption: Single and multi-component systems. *Process Safety and Environmental Protection*, **107**:486–497, 2017. https://doi.org/10.1016/j.psep.2017.03.017.

[10] L. Largitte and R. Pasquier. A review of the kinetics adsorption models and their application to the adsorption of lead by an activated carbon. *Chemical Engineering Research and Design*, **109**:495–504, 2016. https://doi.org/10.1016/j.cherd.2016.02.006.

[11] R. Ocampo-Perez, R. Leyva-Ramos, P. Alonso-Davila, J. Rivera-Utrilla and M. Sanchez-Polo. Modeling adsorption rate of pyridine onto granular activated carbon. *Chemical Engineering Journal*, **165**(1):133–141, 2010. https://doi.org/10.1016/j.cej.2010.09.002.

[12] V. Russo, R. Tesser, D. Masiello, M. Trifuoggi and M. Di Serio. Further verification of adsorption dynamic intraparticle model (ADIM) for fluid-solid adsorption kinetics in batch reactors. *Chemical Engineering Journal*, **283**:1197–1202, 2016. https://doi.org/10.1016/j.cej.2015.08.066.

[13] V. Russo, R. Tesser, M. Trifuoggi, M. Giugni and M. Di Serio. A dynamic intraparticle model for fluid-solid adsorption kinetics. *Computers and Chemical Engineering*, **74**:66–74, 2015. https://doi.org/10.1016/j.compchemeng.2015.01.001.

[14] V. Russo, M. Trifuoggi, M. Di Serio and R. Tesser. Fluid-solid adsorption in bach and continuous processing: a review and insights into modeling. *Chemical Engineering Technology*, **40**(5):799–820, 2017. https://doi.org/10.1002/ceat.201600582.

[15] J.M. Sanz-Serna and S. Larsson. Shadows, chaos, and saddles. *Applied Numerical Mathematics*,**13**:181–190,1993. https://doi.org/10.1016/0168-9274(93)90141-D.

[16] P.R. Souza, G.L. Dotto and N.P.G. Salau. Detailed numerical solution of pore volume and surface diffusion model in adsorption systems. *Chemical Engineering Research and Design*, **122**:298–307, 2017. https://doi.org/10.1016/j.cherd.2017.04.021.

[17] H.H. Tran, F.A. Roddick and J.A. O'Donnell. Comparison of chromatography and desiccant silica gels for the adsorption of metal ions–I. adsorption and kinetics. *Water Research*, **33**(13):2992–3000, 1999. https://doi.org/10.1016/S0043-1354(99)00017-2.